



Diversifying the chloroquinoline scaffold against SARS-CoV-2 main protease: Virtual screening approach using cross-docking, SiteMap analysis and molecular dynamics simulation

MOHAMED AISSAOUI^{1*}, BILLEL BELHANI¹, ABDELMOUMEN BOULEBNANE²,
ABDESLEM BOUZINA¹ and SALAH EDDINE DJILANI³

¹Laboratory of Applied Organic Chemistry, Synthesis of Biomolecules and Molecular Modelling Group, Department of Chemistry, Sciences Faculty, Badji-Mokhtar-Annaba University, Box 12, 23000 Annaba, Algeria, ²Department of English, University of Algiers 2, Abou El Kacem Saâdallah, Algiers, Algeria and ³Laboratory of Synthesis and Organic Biocatalysis, Department of Chemistry, Badji-Mokhtar-Annaba University, Algeria

(Received 17 October, revised 3 December 3 2022, accepted 11 January 2023)

Abstract: The absence of designated remedies for coronavirus disease 19 (Covid-19) and the lack of treatment protocols drove scientists to propose new small molecules and to attempt to repurpose existing drugs against various targets of severe acute respiratory syndrome coronavirus 2 (SARS-CoV-2) in order to bring forward efficient solutions. The main protease (M^{pro}) is one of the most promising drug targets due to its crucial role in fighting viral replication. Several antiviral drugs have been used in an attempt to overcome the pandemic, such as hydroxychloroquine (HCQ). Despite its perceived positive outcomes in the beginning of the disease, HCQ was associated with several drawbacks, such as insolubility, toxicity, and cardiac adverse effects. Therefore, in the present study, a structure-based virtual screening approach was performed to identify structurally modified ligands of the chloroquinoline (CQ) scaffold with good solubility, absorption, and permeation aimed at eventually suggesting a more dependable alternative. PDB ID:7BRP M^{pro} was chosen as the most reliable receptor after cross-docking calculation using 30 crystal structures. Then, a SiteMap analysis was performed and a total of 231,456 structurally modified compounds of the CQ scaffold were suggested. After Lipinski criteria filtration, 64,312 molecules were docked and their MM-GBSA free binding energy were calculated. Next, ADME descriptors were calculated, and 12 molecules with ADME properties better than that of HCQ were identified. The resulting molecules were subjected to molecular dynamics (MD) simulation for 100 ns. The results of the study indicate that 3 molecules (CQ_22; CQ_2 and CQ_5) show better interactions and stability with the M^{pro} receptor.

*Corresponding author. E-mail: mohamed.aissaoui@univ-annaba.dz
<https://doi.org/10.2298/JSC221017003A>

Binding interaction analysis indicates that GLU143, THR26, and HIS41 amino acids are potential binding hot-spot residues for the remaining 3 ligands.

Keywords: COVID19; M^{pro} receptor; structure-based approach; ADME; MM-GBSA.

INTRODUCTION

Since the outbreak of the Covid-19 disease starting from Wuhan city in China, in December 2019, it has been rapidly spreading worldwide and was declared a global health emergency pandemic by the World Health Organization (WHO).¹ Consequently, there was an urgent need for therapeutic strategies to develop antiviral drugs and vaccines that can eradicate this highly contagious virus. This pandemic represents a real threat to global public health and has already infected millions of people leading to a great number of deaths worldwide. The number of casualties is continually increasing at the time of writing this manuscript.^{2,3}

Coronaviruses (CoVs) are large-sized enveloped viruses with a spherical shape, holding single-stranded RNA of positive-sense.⁴ SARS-CoV2 is a novel strain of coronavirus that shares 79.5 % of genomic sequence similarity to SARS-CoV.⁵ The coronavirus has a crown shape that contains four structural proteins.⁶ These proteins are the spike (S) surface glycoprotein, the non-glycosylated envelope (E) protein, the membrane (3CLpro, or M^{pro}) protein, and the nucleoprotein (N) protein. The infection triggers when the Spike protein of the SARS-CoV-2 (COVID-19) interacts with the ACE2 (angiotensin-converting enzyme 2) by TMPRSS2 protease.^{7–9}

The M^{pro} is considered one of the most interesting therapeutic targets in CoVs, as a result of its crucial function in processing the polyproteins that are translated from the viral RNA.¹⁰ These viral polyproteins are cleaved by a proteolysis process to numerous useful proteins.¹¹ Since the M^{pro} cleaves at 11 sites to produce smaller proteins for viral replication, and because of its non-similarity to human proteins, makes the M^{pro} a potential target in anti-Covid-19 drug design.^{12–14}

Since the Covid-19 outbreak, several antiviral drugs have been considered for the treatment of the disease, but their clinical uses were limited due to quality-related safety issues¹⁵ such as Remdesivir¹⁶ and the antimalarial drug hydroxychloroquine (HCQ)/Chloroquine(CQ), Fig. 1.^{17–19}

These drugs were massively used across different countries and were authorised as part of national emergency use programmes and clinical trials by the US Food and Drug Administration (FDA) along with the European Medicines Agency (EMA) for patients affected by SARS-CoV-2 pneumonia.²⁰

Despite being less toxic than CQ, HCQ was found to be a potent inhibitor against SARS-CoV-2 *in vitro*.⁵ However, this drug was associated with several

downsides such as insolubility, toxicity and instability. Moreover, increasing concerns arose when these drugs were used on patients with Covid-19, whether by administering them alone or in combination with other drugs, as a result of cardiac and neuropsychiatric adverse effects.^{21,22} Substantial randomised trials have overpowered features of CQ along with HCQ for Covid-19 effects and there is continued worry about the effects that these treatments may have on patients, whether they have Covid-19 or not.^{23–25}

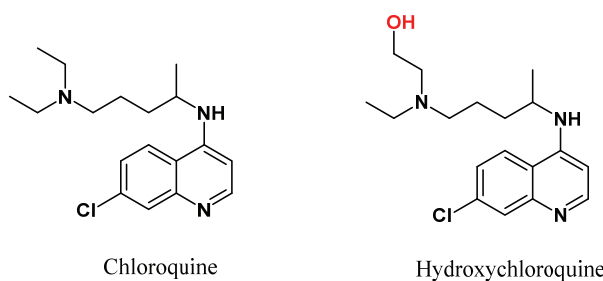
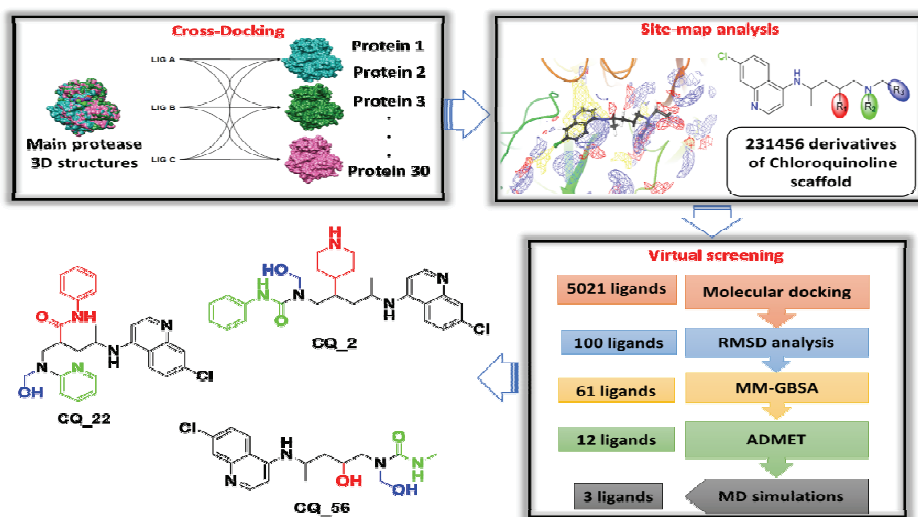


Fig. 1. Chemical structures of chloroquine and hydroxychloroquine.

Aiming towards bringing forth a more reliable and safer substitute for HCQ, in the present study a virtual screening (VS) based drug repurposing method was performed to identify structurally modified compounds of the CQ scaffold with good solubility, absorption, permeation, non-toxic and non-carcinogenic characteristics compared to the parent molecule (HCQ). Drug repurposing is a process of exploring new uses for already existing drugs. It can be a cost-saving and quick strategy as new drug discovery can take numerous years.^{26,27}

Considering computational studies, molecular docking play a major role in the identification and screening of hit molecules and the pathway involved in their mechanism of action. Several *in silico*-based virtual screening studies were conducted for the identification of potential hit molecules.^{28–30}

Accordingly, in this study, Covid-19 M^{pro} crystal complexes available in the PDB were thoroughly explored by cross-docking in order to identify the most reliable PDB structure among them that resulted in PDB ID: 7BRP (Fig. S-1 of the Supplementary material to this paper) as the most appropriate one.³¹ Thereafter, SiteMap analysis was undertaken to better explore the active site of M^{pro} followed by VS and then the molecular docking phase. The absorption, distribution, metabolism and excretion (ADME) properties were calculated and the top-scoring compounds were identified as potential M^{pro} inhibitors. Finally, filtered hits with drug-like properties were used for running molecular dynamics (MD) simulations. A systematic approach based on structure-based drug designing was used in this study as described in Scheme 1.



Scheme 1. Schematic representation of the study design illustration.

MATERIAL AND METHODS

Computing system

The VS workflow and analysis were performed on Centos 7.7 x86-64 (Dell Optiplex 7010). The software that were used in this study were Maestro Schrodinger Release 2018-4 (Maestro, Schrödinger, LLC, New York, NY, 2018) and Chimera 1.15.³²

Cross-docking and protein selection

The three-dimensional structures of 30 M^{pro} targets were retrieved from RCSB PDB.³³ Each protein was prepared using the protein preparation wizard in Maestro.³⁴ The protein structure was integrity adjusted, and the missing side-chain atoms within the protein residues were predicted by Prime.³⁵ Hydrogen atoms were added after deleting ions, cofactors and water molecules. The α -carbons of the structures for each target were aligned to each other using a reference structure; then, each ligand was docked into all 30 structures of the target from which the ligand was extracted (Fig. S-2 of the Supplementary material).

Both the docking reliability and protein selection were evaluated by calculating the root-mean-square deviation (*RMSD*) between the crystallized position of the ligand and that predicted by the docking software in the various target structures. The evaluation was performed for both ligands and proteins structures. The XP (extra precision) docking mode included in Glide (grid-based ligand docking with energetics) module of Maestro was selected as the docking protocol in the next steps of virtual screening, with a docking score value of HCQ equal to 22.21 kJ mol⁻¹.

SiteMap analysis

A SiteMap analysis for the docked complex of the M^{pro} HCQ was performed to understand the structure and to exploit the different regions of the active site of the protein in interaction with HCQ. The analysis was performed using the SiteMap module of Schrodinger.³⁶

Data set generation and preparation

Using CombGlide,³⁷ a data set of 231,456 CQ derivatives was generated by creating 3 sites of substitutions on the HCQ structure. The preparation of the ligands was carried out utilizing the LigPrep module of the Schrodinger Suite.³⁸ The OPLS3 force field was selected for energy minimization.³⁹ All possible protonation and ionization states including stereochemistry, tautomers and ring conformations were generated. A maximum of 32 stereoisomers per ligand were taken into account when creating stereoisomers. For each ligand, only the conformation with the lowest energy was retained. Through Lipinski Ro5 (rule of five) filtration using QikProp,⁴⁰ a module of the Schrödinger software suite, only 64132 CQ derivatives with drug-likeness property were selected for the virtual screening study.

Virtual screening workflow

In order to identify the appropriate compounds that perfectly fit the binding site of the M^{pro}, the above selected derivatives were considered for a virtual screening study. The selected database was initially screened with molecular docking calculations. Only 5021 ligands were selected with an acXP-docking score $\geq 22.21 \text{ kJ mol}^{-1}$. The ones that succeeded were ranked based on the *RMSD* value compared to the HCQ reference structure. Only 100 ligands with a *RMSD* value $\leq 0.2 \text{ nm}$ were kept. The Prime MM/GBSA (molecular mechanics/ Poisson–Boltzmann generalized born surface area) was used to rank the best compounds; 71 ligands with MM/GBSA values comparable to or greater than that of the standard ligand (HCQ) were selected. Additionally, a variety of key ADME properties were also calculated with the aid of QuikProp, taking oral absorption as the primary filtering criterion. Therefore, 12 ligands with oral absorption $\geq 80\%$ were subjected to molecular dynamics simulations (MD). Finally, to validate the accuracy of the results and the stability of the selected ligands, MD simulations were conducted using Desmond.⁴¹ The simulation started by solvating the complex using the TIP3P water model (transferable intermolecular interaction potential 3) with an orthorhombic box of $1\times 1\times 1 \text{ nm}^3$. The system was made electrically neutral by adding appropriate counter ions. OPLS3 force field parameters were utilized for the simulations study. The model systems were relaxed before the simulations. The simulation was then performed using an NPT ensemble system with 300.0 K temperature and 10^5 Pa pressure. The complexes were subjected to molecular dynamics simulation for 100 ns. The *RMSD* of the proteins and ligands was used to assess the stability over time of simulation.

RESULTS AND DISCUSSION

Cross-docking and docking protocol validation

In order to validate both the docking reliability and protein selection in terms of qualitative prediction of the ligand-binding site disposition, 30 M^{pro} targets were considered. Through cross-docking for all complexes, the ligands were extracted from their X-ray complex and subjected to a conformational search. They were then docked in all the structures of the same target using the glide XP docking method and the obtained docking results were compared with the experimentally determined ligand dispositions (co-crystallized ligand) taking into account the average root-mean-square deviation (*RMSD*) as the principal parameter. The main results obtained from the cross-docking studies are summarized in Fig. S-3 of the Supplementary material. The M^{pro} protein with PDB ID:7BRP seemed to be the best performing receptor with an *RMSD* of 0.27 nm. Based on this ana-

lysis, the 7BRP receptor was selected in the next stage of this study. The 3D crystal structure of the 7BRP receptor has a resolution of 0.180 nm, a structural weight of 68.81 kDa and amino acid length of 307 and it contains two chains.⁴²

SiteMap analysis and dataset creation

The SiteMap analysis was realized using the M^{pro} PDB ID: 7BRP receptor in the complex with HCQ after docking calculation by the Glide-XP method. The SiteMap results are summarized in Table I with a SiteScore of 0.946.

Understanding the interaction of the HCQ in the active site using SiteMap analysis revealed the presence of two principal regions, the first was a hydrophilic region with ligand hydrogen-bond donors and acceptors interactions (Fig. S-4a of the Supplementary material) representing a hydrophilic-score of 0.563, the second was the hydrophobic region occupied by the chloroquinoline moiety that seemed to be suitable for occupancy by this hydrophobic group (Fig. S-4b) with a hydrophobic-score of 0.442.

TABLE I. Summary results of SiteMap analysis using M^{pro}-HCQ complex; SiteScore: the SiteScore is based on a weighted sum of several properties as the number of site points; Dscore: druggability score, uses the same properties as SiteScore but with different coefficients; Phobic: hydrophobic region score; philic: hydrophilic region scores

Site	SiteScore	Size	Dscore	Volume	Contact	Phobic	Philic
Sitemap_site_1	0.946	387	1.044	290.178	0.501	0.442	0.563

The suggested strategies of this study can provide insights into HCQ-M^{pro} interactions to propose an effective modification on the CQ scaffold. After analysis, where modifications on CQ scaffold would be expected to promote the binding mode was revealed. Therefore, 3 substitution sites were suggested (R₁, R₂ and R₃) and a data set of 231,456 molecules based on the CQ scaffold were designed and computationally optimized (Fig. 2).

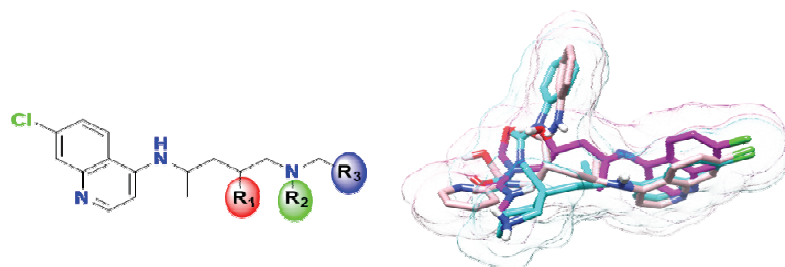


Fig. 2. The proposed chemical structure of the chloroquinoline scaffold.

These molecules were designed by substituting different groups with different characteristics at the positions R₁, R₂ and R₃. The VS methodology using molecular docking, Lipinski Ro5 filtration, as well as MM-GBSA, ADME and

MD simulation were employed to identify the ligands having a better affinity for the M^{pro} protein of SARS-CoV-2.

Virtual screening strategy

Lipinski Ro5 filtration. As the first step of the VS workflow, the 231,456 generated derivatives were subjected to Lipinski's Ro5 filtrations, such as molecular weight, H-bond donor/acceptor and octanol/water partition coefficient (*QPlogPo/w*). Only 64,132 derivatives with drug-likeness property were selected. The docking results of the 64,132 modified CQ scaffold against M^{pro} were examined. As hydroxychloroquine potently inhibits viral infection of SARS coronavirus (SARS-CoV-1),⁴³ the binding mode of this compound was taken as a reference structure in the next stage of docking calculation. All 64,132 ligands were inspected based on their docking score and the ones showing a docking score $\geq 22.21 \text{ kJ mol}^{-1}$ were chosen. Therefore, 5021 ligands were selected. To choose ligands that maintain the same binding mode of HCQ inside the active site, *RMSD* values were calculated between the docked HCQ pose and the remaining 5021 ligands poses using the 'superimpose' module. Finally, 100 ligands having the same binding mode as HCQ with a *RMSD* value of $\leq 0.2 \text{ nm}$ were kept.

MM-GBSA study. The stability of the ligand after binding to the active site of the enzyme was confirmed by MM-GBSA analyses computation. All 100 ligands were subjected to calculation of the ligand-receptor binding energy. After MM-GBSA analysis, only 71 ligands with binding energy better than HCQ (Table S-I of the Supplementary material), were submitted to an accurate prediction of their ADME properties

ADME analysis. The ADME properties of the last selected derivatives (71 ligands) were calculated. As the ligands had previously passed through Lipinski Ro5 filtration, it could be predicted that the selected ligands obeyed Lipinski's Ro5 and are likely to be orally active. Hence, these ligands were screened through a variety of key ADME properties based on oral absorption as a primary filtering criterion. Only 13 ligands with oral absorption comparable to or greater than 80 % were selected. The remaining ligands were following the standard parameters and the results are shown in Table II. Finally, ADME property analysis concluded that the final screened ligands show drug-likeness properties.

MD simulation. The simulations were performed to gain more insight into the stability of the ligand–protein complex. The results of the MD simulations were examined based on the *RMSD* of both, the protein backbone (C α atoms) and the ligand of interest. The protocol was further validated using the crystal structure of M^{pro} (PDB ID:7BRP) complexed with HCQ as the reference structure. MD simulations were processed for 100 ns. The *RMSD* plot for C α (in blue) complexed with HCQ was observed to be in the range of 0.10–0.20 nm (Fig. 3a),

this result clearly reveals that the presence of HCQ in the active site of protein kept it stable throughout the simulation time.

TABLE II. ADME properties of HCQ and all 13 ligands to determine their “drug-likeness”; *PSA*: van der Waals surface area of polar nitrogen and oxygen atoms (acceptable range : 7.0–200.0); *dHB*: estimated hydrogen bonds that could be donated (acceptable range: 0.0–6.0); *aHB*: estimated hydrogen bonds that could be accepted (acceptable range: 2.0–20.0); *QPlogS*: predicted aqueous solubility (acceptable range: -6.5–0.5); *QPlogPo/w*: predicted octanol/water partition coefficient (acceptable range: -2.0–6.5); *QPPCaco*: predicted apparent Caco-2 cell permeability in nm/s (< 25 poor and >500 great); *QPlogBB*: predicted brain/blood partition coefficient (acceptable range: -3.0–1.2); *PHOA*: percent human oral absorption (80 % is high and 25 % is low); *RO5*, number of violations of the Lipinski rule of five (maximum is 4; in all cases found 0)

Title	<i>MW</i> g mol ⁻¹	<i>PSA</i> nm ²	<i>dHB</i>	<i>aHB</i>	<i>QPlogS</i> mol dm ⁻³	<i>QPlogPo/w</i>	<i>QPPCaco</i>	<i>QPlogBB</i>	<i>PHOA</i> %
H_CQ	335.876	0.48946	2	5.7	-3.385	3.265	383.503	-0.322	90.308
CQ_7	442.947	0.80245	1	9.4	-4.761	3.807	836.988	-1.262	100.000
CQ_10	499.008	1.07465	3	9.4	-4.724	3.745	513.809	-1.291	100.000
CQ_22	490.003	0.85299	3	7.7	-5.635	4.409	1409.075	-0.921	100.000
CQ_56	366.847	1.00931	3	6.4	-3.517	2.303	222.546	-1.303	100.000
CQ_2	496.051	0.91490	3	6.2	-5.455	4.604	97.758	-0.890	100.000
CQ_15	427.933	0.89329	3	8.7	-4.518	2.976	793.489	-0.947	96.267
CQ_49	470.013	0.81156	3	9.4	-4.321	3.611	248.735	-0.647	90.968
CQ_52	385.895	0.79992	4	7.2	-4.444	3.299	206.815	-0.759	87.706
CQ_64	425.911	1.02547	3	9.6	-4.077	3.412	138.152	-1.394	85.229
CQ_42	401.895	1.11224	2	8.5	-3.974	2.329	295.147	-1.351	84.791
CQ_43	401.895	1.11224	2	8.5	-3.974	2.329	295.147	-1.351	84.791
CQ_53	441.962	0.96928	3	8.7	-3.560	3.121	100.413	-1.150	81.049
CQ_14	480.054	0.81486	2	9.0	-3.909	4.021	49.230	-0.615	80.777

The Ligand–RMSD plot for HCQ (in red) was found in the range of 0.05 to 0.48 nm with a little fluctuation during initial time of simulation. However, it gradually attained stability towards the end of the simulation with an *RMSD* of 0.18 nm. The graph of Ligand–RMSD specifies that the M^{pro}–HCQ complex is stable during the MD simulation time and the HCQ ligand constantly maintained its interactions with the receptor during the whole simulation.

The 13 compounds selected through the VS study were subjected to the same MD simulations protocol described above. The *RMSD* of their disposition during the simulation compared to their initial docking pose was calculated and the stability of the interactions predicted by docking calculations were analysed. Only compounds showing an average *RMSD* < 0.3 nm and maintained at least one H-bond with the receptor for more than 70 % of the whole MD simulation were then retrieved.

Applying this restriction, 10 compounds were rejected and the remaining 3 compounds, CQ_22, CQ_2 and CQ_56 (Fig. 4) were considered for 3D inter-

action analysis due to their stability during MD simulations (Fig. 3b, c and d). A summary of structure-based VS strategy is provided in Table III.

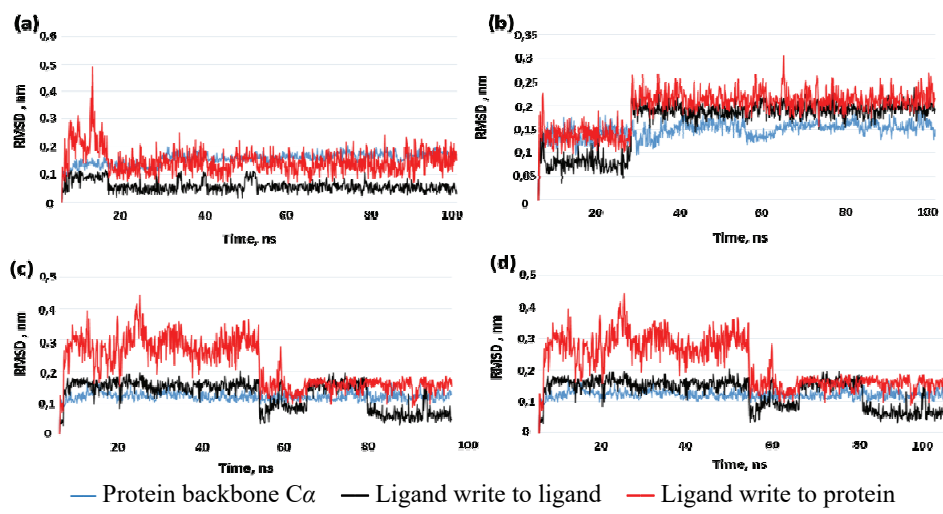


Fig. 3. The RMSD graphs obtained after MD analysis of: a) HCQ; b) CQ_22; c) CQ_2; d) CQ_56.

TABLE III. Mpro residue interactions, docking score and energy of HCQ and the 3 hits

Title	Docking score, kJ mol ⁻¹	Glide energy kJ mol ⁻¹	Glide model, kJ mol ⁻¹	Residual interactions		
				H-bond	$\pi-\pi$ stacking	Hydrophobic
H_CQ	-22.24	-170.47	-196.09	CYS145, SER144	HIS41	MET165, MET49
CQ_22	-23.89	-261.30	-363.50	THR26, GLY143	HIS41	VAL186, MET49
CQ_2	-22.30	-244.09	-300.19	THR26, CYS145, GLY143	HIS41	MET165, PHE140, VAL186,
CQ_56	-27.16	-215.89	-281.72	HIS164, ASN142, GLY143, THR26	HIS41	MET165, MET49

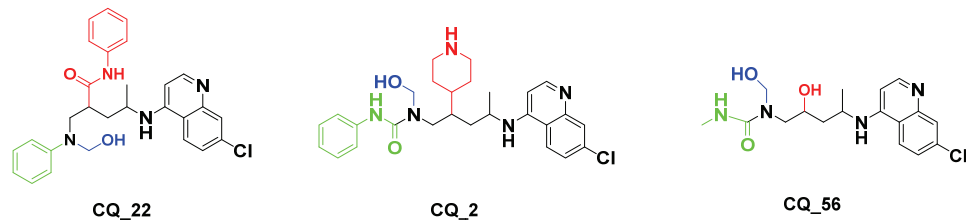


Fig. 4. 2D Structure of the 3 selected hits.

The root mean square fluctuation (*RMSF*) value of macromolecular residues for the 3 complexes was determined to be well within the allowed range of 0.3 nm. A few residues changed slightly, with an *RMSF* values of 0.2–0.3 nm. However, the bulk of residues exhibited smaller variations, with an average value of less than 0.1 nm as shown in Fig. S-5 of the Supplementary material. The observed *RMSF* of the 3 ligands complex within the M^{pro} binding site was found to be within the range. The observed *RMSF* of the 3 ligands (CQ_22, CQ_2 and CQ_56) complex within the active binding site of the M^{pro} enzyme was found to be within the range of 0.09–0.25 nm throughout the 100 ns simulation time as shown in Fig. S-6 of the Supplementary material. This clearly indicates that the ligands were stabilized within the active site with minor functional fluctuations that are required for interacting with the target macromolecule.

The interactions made by ligands CQ_22, CQ_2 and CQ_56 with M^{pro} enzyme are given in Fig. S-7 of the Supplementary material in which the interaction types with their percentages during 100 ns MD simulation run are represented. Histograms represent the interaction fraction of these ligands. Hydrogen bonds, hydrophobic interactions such as π cation, π – π stacking, water bridges and ionic interactions made by ligand with amino acids of proteins during 100 ns MD simulation are represented in Fig. S-7. For all the histograms in Fig. S-7, the stacked bar histograms are normalised over the course of the trajectory; for example, a value of 0.8 suggests that 80 % of the simulation time of the specific interaction is maintained. Values over 1.0 are possible as some protein residue may make multiple contacts of the same subtype with the ligand. All the histogram bars suggest that all the ligands (CQ_22, CQ_2 and CQ_56) form strong interactions with several amino acids of M^{pro}. In several instances, the interaction fraction shoots above the value of 0.7, which shows strong interaction of ligands with that amino acid.

Binding interactions analysis of Mpro_HCQ complex

In this investigation, the function of amino acids within the M^{pro} active site evaluated. Therefore, a molecular interaction study was performed and HCQ binding mode interaction was taken as reference. As shown in Fig. S-8 of the Supplementary material, the binding mode analysis of HCQ with M^{pro} showed the presence of hydrogen bond interactions as well as hydrophobic interactions. The terminal hydroxyl group of the HCQ made two H-bonds as an acceptor with SER144 and CYS145. The quinoline ring of HCQ displayed π – π stacking interactions with HIS41, and hydrophobic interactions with MET165; MET49 and VAL186.⁴⁴

Binding interactions analysis of the Mpro_CQ22, CQ_2 and CQ_56 complexes

Docking results showed that the CQ_22 molecule was mainly combined with M^{pro} through three H-bonds. The first as a donor through the hydroxyl

group with THR26, the second exhibited by the pyrimidine nitrogen as an acceptor with the same residue, and the last as an acceptor with GLY143 through the carbonyl group. Moreover, favourable conventional interaction was displayed by the quinoline ring as π - π stacking interaction with HIS41. Hydrophobic interactions with VAL186, and MET49 were also present, as shown in Fig. 5a.

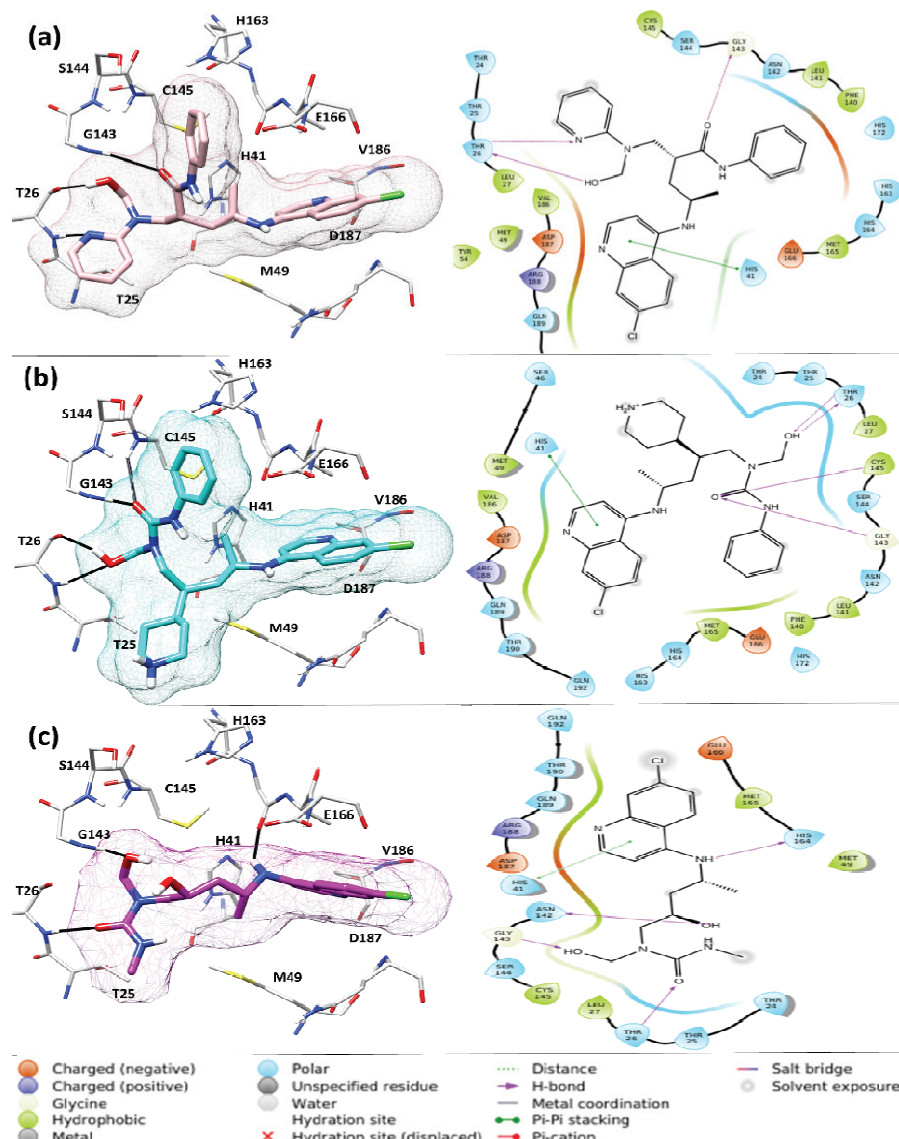


Fig. 5. Binding disposition of selected ligands after docking calculations in the active site of M^{pro}: a) CQ_22 in pink sticks; b) CQ_2 in cyan sticks; c) CQ_56 in magenta sticks. H-bonds are shown as black lines.

Considering CQ_2, four H-bonds were formed; one among them was similar to the HCQ with CYS145 as an acceptor through the carbonyl group. The same carbonyl group formed a hydrogen bond with GLY143. The two-remaining H-bonds were exhibited by hydroxyl group with THR26 as acceptor and donor simultaneously. The presence of $\pi-\pi$ stacking conventional interaction through quinoline ring with HIS41 was noted (Fig. 5b).

Compound CQ_56 showed four H-bonds; the first through the amino group, located at the fourth position with HIS164 as a donor group. The second as a donor with ASN142 through the hydroxyl, located at the second position. The last two H-bonds as acceptor with GLY143 and THR26 through hydroxyl and carbonyl groups, respectively. Likewise, $\pi-\pi$ stacking conventional interaction through the quinoline ring with HIS4 was present (Fig. 5c). The ligand–amino acid interaction of residue HIS41 always took place in all the 3 stable ligands through $\pi-\pi$ stacking interactions with the quinoline ring.

In addition, common H-bound interactions were detected with GLY143 and THR26 residues, when these compounds have substituent with acceptor and donor character in that region (hydrophilic region, Fig. S-4), which is not the case in the HCQ molecule. This suggests that the presence of a hydrogen bond interaction with both GLY143 and THR26 may improve the stability within the M^{Pro} active site. Therefore, the docking results indicate that GLY143, THR26 and HIS41 amino acids in the binding pocket are potential binding hot-spot residues for our ligands. Additionally, the presence of substituents with acceptor and donor characters in the hydrophilic region improves the stability and the interaction mode of the molecules.

CONCLUSIONS

The Covid-19 pandemic caused a global health crisis worldwide leading to many casualties. The constant mutations of the virus jeopardized the effectiveness of vaccines as a distinct solution. This emphasized the need for therapeutic drugs that target and inhibit the replication of the virus. Drug repurposing is considered as an important strategy in fighting the pandemic considering the urgency of the health situation given that the traditional process of developing targeted drug can take a long time. HCQ was considered by research organizations as a potential drug against the coronavirus during the early days of the pandemic. However, the lack of sufficient evidence of its usefulness along with some adverse effects lead the WHO to eventually revoke the drug. Thus, the present study attempts to conduct a structure-based VS approach to discover a new modified CQ scaffolds able to affect the Sars-CoV2 M^{Pro} that may be more effective and reliable alternatives. The results of the study show that CQ_22, CQ_2 and CQ_56 molecules demonstrate better docking scores (-5.712 , -5.332 and -6.493 , respectively) as well as better ADME properties in comparison to HCQ. Analysis

of the binding interactions of the selected ligands shows that within the active substrate binding pocket of M^{pro}, HIS41, THR26 and GLY143 are the specific amino acid residues involved in interaction with target molecules. This emphasizes their significance as key residues capable of facilitating substrate-ligand complex formation and modulating the M^{pro} enzyme function as potential inhibitors. The presented data may provide some insights into the development of novel potent M^{pro} inhibitors and hold promise for new potential SARS-CoV-2 drugs.

SUPPLEMENTARY MATERIAL

Additional data and information are available electronically at the pages of journal website: <https://www.shd-pub.org.rs/index.php/JSCS/article/view/12105>, or from the corresponding author on request.

Acknowledgments. The authors would like to thank The General Directorate for Scientific Research and Technological Development (DG-RSDT), the Algerian Ministry of Scientific Research, Applied Organic Chemistry Laboratory (FNR 2000).

ИЗВОД

ДИВЕРЗИФИКАЦИЈА СКЕЛЕТА ХЛОРОХИНОЛИНА ЗА БЛОКИРАЊЕ ГЛАВНЕ ПРОТЕАЗЕ SARS-CoV-2: ПРИСТУП ВИРТУАЛНИМ СКЕНИРАЊЕМ КОРИСТЕЋИ CROSS-DOCKING, SITEMAP АНАЛИЗУ И СИМУЛАЦИЈУ МОЛЕКУЛСКОМ ДИНАМИКОМ

МОХАМЕД АИССАУІ¹, БИЛЕЛ БЕЛХАНИ¹, АБДЕЛМОУЕН БУЛЕБНАНЕ², АБДЕСЛЕМ БУЗИНА¹ и САЛАХ ЕДДИН ДЖИЛАНІ³

¹Laboratory of Applied Organic Chemistry, Synthesis of Biomolecules and Molecular Modelling Group, Department of Chemistry, Sciences Faculty, Badji-Mokhtar-Annaba University, Box 12, 23000 Annaba, Algeria, ²Department of English, University of Algiers 2, Abou El Kacem Saâdallah, Algiers, Algeria and

³Laboratory of Synthesis and Organic Biocatalysis, Department of Chemistry, Badji-Mokhtar-Annaba University, Algeria

Одсуство одређених лекова за болест корона вируса 19 (Covid-19) и немање прототипа за третирање, навело је научнике да предложе нове мале молекуле и да покушају постојеће лекове да пренамене против различних циљаних тешких респираторних синдрома коронавируса 2 (SARS-CoV-2) и дођу до ефикасних решења. Главна протеаза (M^{pro}) је једна од највише обећавајућих мета лекова због своје кључне улоге у борби против репликације вируса. Неколико антивирусних лекова је коришћено у покушају да се превазиђе пандемија, попут хидроксихлорокина (HCQ). Упркос опаженим позитивним исходима у почетку болести, HCQ је повезан са неколико недостатака попут нерастворљивости, токсичности и нежелених ефеката на срце. Зато, у овој студији, урадили смо на-структурни-заснован виртуални скрининг да би идентификовали структурно модификоване лиганде хлорохинолинског (CQ) скелета који имају добру растворљивост, апсорпцију и прожимање у циљу евентуалног суперисања поузданije алтернативе. PDB ID:7BRP M^{pro} је изабран као најпоузданiji рецептор након cross-docking израчунавања користећи 30 кристалних структура. Онда је урађена SiteMap анализа и предложено је укупно 231456 структурно модификованих једињења са CQ скелетом. Након филтрирања са критеријума Липинског, 64312 молекула је доковано и израчунате су њихове MM-GBSA слободне енергије везивања. Затим су израчунати њихови ADME дескриптори, и идентификовано је 12 молекула са ADME својствима бољим од HCQ. Ти молекули су подвргнути симулацији молекулском динамиком (MD) за 100 ns. Резултати сту-

дије показују да три молекула (CQ_22; CQ_2 и CQ_56) показују бољу интеракцију и стабилност са M^{pro} рецептором. Везивне интеракције указују да су GLU143, THR26 и HIS41 амино киселине потенцијалне вруће тачке за преостала 3 лиганда.

(Примљено 17. октобра, ревидирано 3. децембра 2022, прихваћено 11. јануара 2023)

REFERENCES

1. S. Ludwig,A. Zarbock, *Anesth. Analg.* **131** (1) (2020) 93
(<https://doi.org/10.1213/ane.0000000000004845>)
2. K. Dhama, S. K. Patel, K. Sharun, M. Pathak, R. Tiwari, M. I. Yatoo, Y. S. Malik, R. Sah, A. A. Rabaan,P.K. Panwar, *Travel. Med. Infect. Dis.* **37** (2020) 101830
(<https://doi.org/10.1016/j.tmaid.2020.101830>)
3. K. Yuki, M. Fujiogi,S. Koutsogiannaki, *Clin. Immunol.* **215** (2020) 108427
(<https://doi.org/10.1016/j.clim.2020.108427>)
4. I. M. Artika, A. K. Dewantari, A. Wiyatno, *Heliyon.* **6** (2020) e04743
(<https://doi.org/10.1016/j.heliyon.2020.e04743>)
5. Y. Zhou, Y. Hou, J. Shen, Y. Huang, W. Martin, F. Cheng, *Cell Discov.* **6** (2020) 14
(<https://doi.org/10.1038/s41421-020-0153-3>).
6. C. Wu, Y. Liu, Y. Yang, P. Zhang, W. Zhong, Y. Wang, Q. Wang, Y. Xu, M. Li, X. Li, M. Zheng, L. Chen,H. Li, *Acta Pharm. Sin. B.* **10** (2020) 766
(<https://doi.org/10.1016/j.apsb.2020.02.008>)
7. J. Shang, Y. Wan, C. Luo, G. Ye, Q. Geng, A. Auerbach,F. Li, *Proc. Natl. Acad. Sci. U.S.A.* **117** (2020) 11727 (<https://doi.org/10.1073/pnas.2003138117>).
8. L. Mousavizadeh,S. Ghasemi, *J. Microbiol. Immunol. Infect.* **54** (2021) 159
(<https://doi.org/10.1016/j.jmii.2020.03.022>)
9. J. Yang, S. J. L. Petitjean, M. Koehler, Q. Zhang, A. C. Dumitru, W. Chen, S. Derclaye, S. P. Vincent, P. Soumillion, D. Alsteens, *Nat. Commun.* **11** (2020) 4541
(<https://doi.org/10.1038/s41467-020-18319-6>)
10. X. Xue, H. Yu, H. Yang, F. Xue, Z. Wu, W. Shen, J. Li, Z. Zhou, Y. Ding, Q. Zhao, X.C. Zhang, M. Liao, M. Bartlam, Z. Rao, *J. Virol.* **82** (2008) 2515
(<https://doi.org/10.1128/JVI.02114-07>)
11. C. Liu, Q. Zhou, Y. Li, L.V. Garner, S.P. Watkins, L .J. Carter, J. Smoot, A. C. Gregg, A. D. Daniels, S. Jersey, D. Albaiu, *ACS Cent. Sci.* **6** (2020) 315
(<https://doi.org/10.1021/acscentsci.0c00272>)
12. M. T. ul Qamar, S. M. Alqahtani, M. A. Alamri,L.-L. Chen, *J. Pharm. Anal.* **10** (2020) 313 (<https://doi.org/10.1016/j.jpha.2020.03.009>)
13. Z. Jin, X. Du, Y. Xu, Y. Deng, M. Liu, Y. Zhao, B. Zhang, X. Li, L. Zhang, C. Peng, Y. Duan, J. Yu, L. Wang, K. Yang, F. Liu, R. Jiang, X. Yang, T. You, X. Liu, X. Yang, F. Bai, H. Liu, X. Liu, L.W. Guddat, W. Xu, G. Xiao, C. Qin, Z. Shi, H. Jiang, Z. Rao, H. Yang, *Nature.* **582** (2020) 289 (<https://doi.org/10.1038/s41586-020-2223-y>)
14. M. Bzówka, K. Mitusińska, A. Raczyńska, A. Samol, J. A. Tuszyński,A. Góra, *Int. J. Mol. Sci.* **21** (2020) 3099 (<https://doi.org/10.3390/ijms21093099>)
15. R. K. Harwansh, S. Bahadur, *Curr. Pharm. Biotechnol.* **23** (2022) 235
(<https://doi.org/10.2174/1389201022666210322124348>)
16. C. Scavone, S. Brusco, M. Bertini, L. Sportiello, C. Rafaniello, A. Zoccoli, L. Berrino, G. Racagni, F. Rossi, A. Capuano, *Br. J. Pharmacol.* **177** (2020) 4813
(<https://doi.org/10.1111/bph.15072>)
17. M. Nimgampalle, V. Devanathan, A. Saxena, *J. Biomol. Struct. Dyn.* **39** (2021) 4949
(<https://doi.org/10.1080/07391102.2020.1782265>)

18. P. Gautret, J. C. Lagier, P. Parola, V. T. Hoang, L. Meddeb, M. Mailhe, B. Doudier, J. Courjon, V. Giordanengo, V. E. Vieira, H. Tissot Dupont, S. Honoré, P. Colson, E. Chabrière, B. La Scola, J. M. Rolain, P. Brouqui, D. Raoult, *Int. J. Antimicrob. Agents* **56** (2020) 105949 (<https://doi.org/10.1016/j.ijantimicag.2020.105949>)
19. M. Wang, R. Cao, L. Zhang, X. Yang, J. Liu, M. Xu, Z. Shi, Z. Hu, W. Zhong, G. Xiao, *Cell Res.* **30** (2020) 269 (<https://doi.org/10.1038/s41422-020-0282-0>)
20. European Medicine Agency, *COVID-19: Chloroquine and hydroxychloroquine only to be used in clinical trials or emergency use programmes*, 2020 (<https://www.ema.europa.eu/en/news/covid-19-chloroquine-hydroxychloroquine-only-be-used-clinical-trials-emergency-use-programmes>)
21. K. Sato, T. Mano, A. Iwata, T. Toda, *Biosci. Trends* **14** (2020) 139 (<https://doi.org/10.5582/bst.2020.03082>)
22. C. Chatre, F. Roubille, H. Vernhet, C. Jorgensen, Y.-M. Pers, *Drug. Saf.* **41** (2018) 919 (<https://doi.org/10.1007/s40264-018-0689-4>)
23. Z. Kashour, M. Riaz, M. A. Garbati, O. Al Dosary, H. Tlayjeh, D. Gerberi, M. H. Murad, M. R. Sohail, T. Kashour, I. M. Tleyjeh, *J. Antimicrob. Chemother.* **76** (2021) 30 (<https://doi.org/10.1093/jac/dkaa403>)
24. X. Cui, J. Sun, S.J. Minkove, Y. Li, D. Cooper, Z. Couse, P. Q. Eichacker, P. Torabi-Parizi, *Rev. Med. Virol.* **31** (2021) e2228 (<https://doi.org/10.1002/rmv.2228>)
25. T. Fiolet, A. Guihur, M. E. Rebeaud, M. Mulot, N. Peiffer-Smadja, Y. Mahamat-Saleh, *Clin. Microbiol. Infect.* **27** (2021) 19 (<https://doi.org/10.1016/j.cmi.2020.08.022>)
26. T. U. Singh, S. Parida, M. C. Lingaraju, M. Kesavan, D. Kumar, R. K. Singh, *Pharmacol. Reports* **72** (2020) 1479 (<https://doi.org/10.1007/s43440-020-00155-6>)
27. A. Khataniar, U. Pathak, S. Rajkhowa, A. N. Jha, *Covid* **2** (2022) 148 (<https://doi.org/10.3390/covid2020011>)
28. D. M. Teli, M. B. Shah, M. T. Chhabria, *Front. Mol. Biosci.* **7** (2021) 599079 (<https://doi.org/10.3389/fmrb.2020.599079>)
29. M. G. Santibáñez-Morán, E. López-López, F. D. Prieto-Martínez, N. Sánchez-Cruz, J. L. Medina-Franco, *RSC Adv.* **10** (2020) 25089 (<https://doi.org/10.1039/D0RA04922K>)
30. R. K. Gupta, E. L. Nwachuku, B. E. Zusman, R. M. Jha, A. M. Puccio, *PLoS ONE* **16** (2021) e0257784 (<https://doi.org/10.1371/journal.pone.0257784>)
31. L. Fu, F. Ye, Y. Feng, F. Yu, Q. Wang, Y. Wu, C. Zhao, H. Sun, B. Huang, P. Niu, H. Song, Y. Shi, X. Li, W. Tan, J. Qi, G. F. Gao, *Nat. Commun.* **11** (2020) 4417 (<https://doi.org/10.1038/s41467-020-18233-x>)
32. E. F. Pettersen, T. D. Goddard, C. C. Huang, G. S. Couch, D. M. Greenblatt, E. C. Meng, T. E. Ferrin, *J. Comput. Chem.* **25** (2004) 1605 (<https://doi.org/10.1002/jcc.20084>)
33. H. M. Berman, J. Westbrook, Z. Feng, G. Gilliland, T. N. Bhat, H. Weissig, I. N. Shindyalov, P. E. Bourne, *Nucleic Acids Res.* **28** (2000) 235 (<https://doi.org/10.1093/nar/28.1.235>)
34. J. C. Shelley, A. Cholleti, L. L. Frye, J. R. Greenwood, M. R. Timlin, M. Uchimaya, *J. Comput. Aided Mol. Des.* **21** (2007) 681 (<https://doi.org/10.1007/s10822-007-9133-z>)
35. M. P. Jacobson, R. A. Friesner, Z. Xiang, B. Honig, *J. Mol. Biol.* **320** (2002) 597 ([https://doi.org/10.1016/S0022-2836\(02\)00470-9](https://doi.org/10.1016/S0022-2836(02)00470-9))
36. T. A. Halgren, *J. Chem. Inf. Model.* **49** (2009) 377 (<https://doi.org/10.1021/ci800324m>)
37. T. A. Halgren, R. B. Murphy, R. A. Friesner, H. S. Beard, L. L. Frye, W. T. Pollard, J. L. Banks, *J. Med. Chem.* **47** (2004) 1750 (<https://doi.org/10.1021/jm030644s>)
38. M. F. Al Ajmi, M. T. Rehman, A. Hussain, G. M. Rather, *Inter. J. Bio. Macromol.* **116** (2018) 173 (<https://doi.org/10.1016/j.ijbiomac.2018.05.023>)

39. E. Harder, W. Damm, J. Maple, C. Wu, M. Reboul, J. Y. Xiang, L. Wang, D. Lupyan, M. K. Dahlgren, J. L. Knight, J. W. Kaus, D. S. Cerutti, G. Krilov, W. L. Jorgensen, R. Abel, R. A. Friesner, *J. Chem. Theory Comput.* **12** (2016) 281 (<https://doi.org/10.1021/acs.jctc.5b00864>)
40. A. O. Fadaka, R. T. Aruleba, N. R. S. Sibuyi, A. Klein, A. M. Madiehe, M. Meyer, *J. Biomol. Struct. Dyn.* **40** (2022) 3416 (<https://doi.org/10.1080/07391102.2020.1847197>)
41. K. J. Bowers, D. E. Chow, H. Xu, R. O. Dror, M. P. Eastwood, B. A. Gregersen, J. L. Klepeis, I. Kolossvary, M. A. Moraes, F. D. Sacerdoti, J. K. Salmon, Y. Shan, D. E. Shaw, in *SC '06: Proceedings of the 2006 ACM/IEEE Conference on Supercomputing*, Tampa, FL, 11–17 Nov. 2006, p. 43 (<https://doi.org/10.1109/SC.2006.54>).
42. L. Fu, F. Ye, Y. Feng, F. Yu, Q. Wang, Y. Wu, C. Zhao, H. Sun, B. Huang, P. Niu, *Nat. Commun.* **11** (2020) 1 (<https://doi.org/10.1038/s41467-020-18233-x>)
43. X. Yao, F. Ye, M. Zhang, C. Cui, B. Huang, P. Niu, X. Liu, L. Zhao, E. Dong, C. Song, S. Zhan, R. Lu, H. Li, W. Tan, D. Liu, *Clin. Infect. Dis.* **71** (2020) 732 (<https://doi.org/10.1093/cid/ciaa237>)
44. H. Rai, A. Barik, Y. P. Singh, A. Suresh, L. Singh, G. Singh, U. Y. Nayak, V. K. Dubey, G. Modi, *Mol Divers.* **25** (2021) 1905 (<https://doi.org/10.1007/s11030-021-10188-5>).